Vertical Structure Content of Polarimetric Radio Occultations (PRO) and Applications to Weather Modeling

F. Joseph Turk[1], Ramon Padulles[2], Estel Cardellach[2], Chi O. Ao[1], Manuel de la Torre-Juarez[1], Kuo-Nung Wang[1], Mayra Oyola[1], J. David Neelin[3], Hui Shao[4], Benjamin Johnson[4]

[1]Jet Propulsion Laboratory, California Institute of Technology, Pasadena CA
[2]ICE-CSIC/IEEC, Barcelona Spain
[3]Dept. of Atmos. & Ocean. Sci., Univ. of California, Los Angeles CA
[4]UCAR/JCSDA, College Park MD

8th International Radio Occultations Working Group Workshop
(IROWG-8)
April 7-9, 11-13, 2021

https://paz.ice.csic.es

Precipitation Climatology

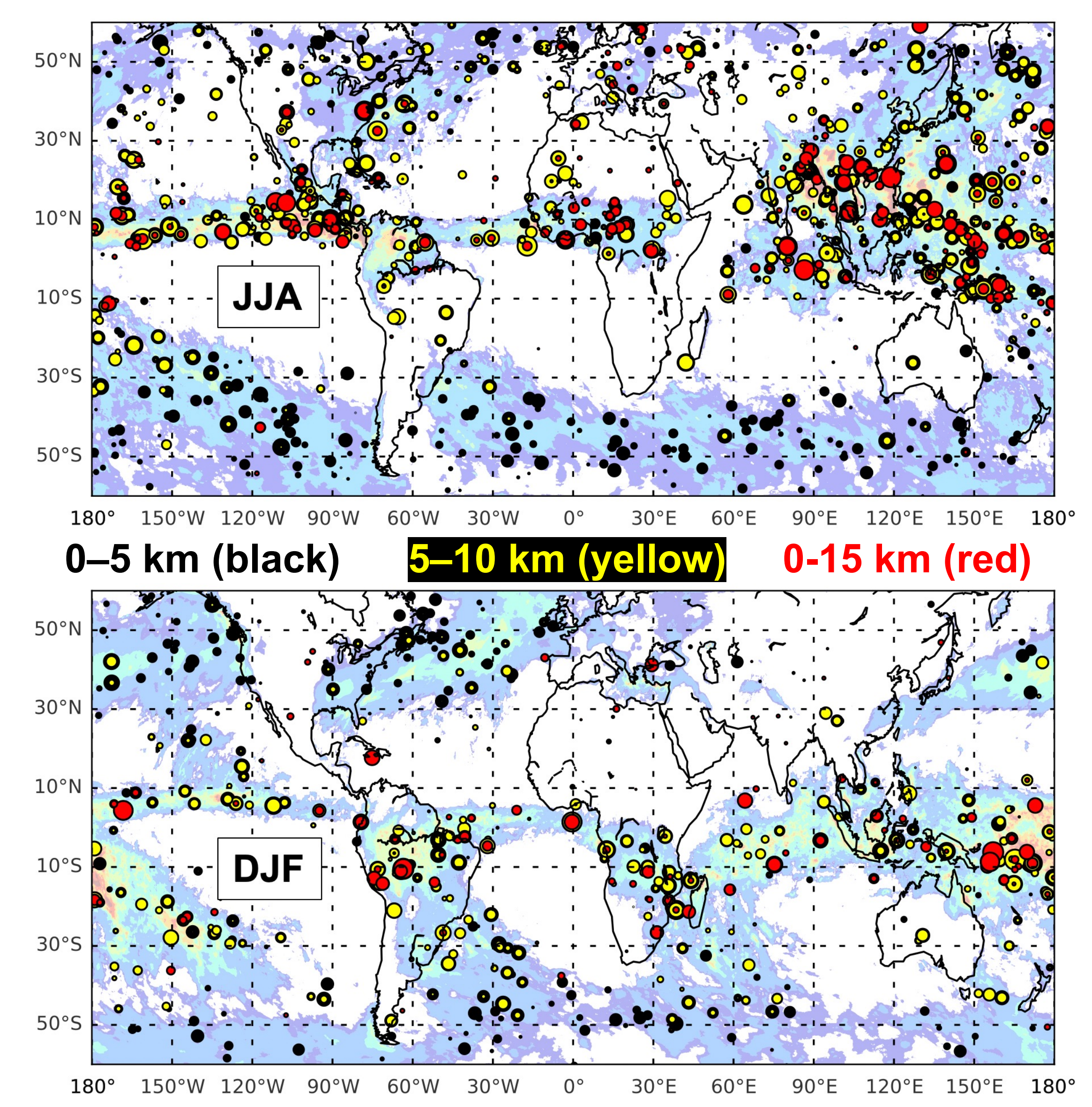

Geographical distribution of the upper percentile (top 2%) of the measured polarimetric phase shift ($\Delta\phi$) from all ROHP observations

Each dot color denotes a vertical region where the $\Delta\phi$ from all rays were averaged

The color contour background is GPM-IMERG averaged over the same 3-month period

Geographical agreement with known global precipitation patterns

$\Delta\phi$ adds an indication of vertical precipitation structure to the (T, q, p) profile

Purpose of this investigation is to characterize the $\Delta\phi$ profile, to facilitate its science usage

Relating Polarimetric Phase Difference to Precipitation Structure

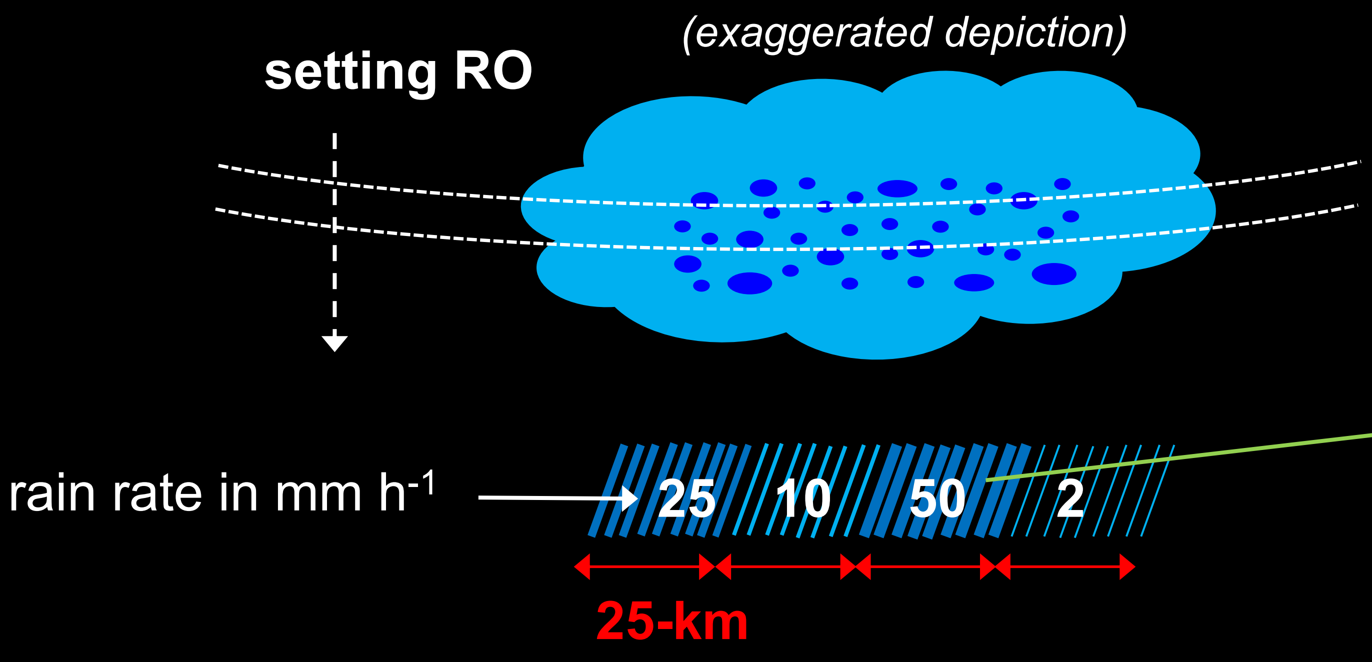

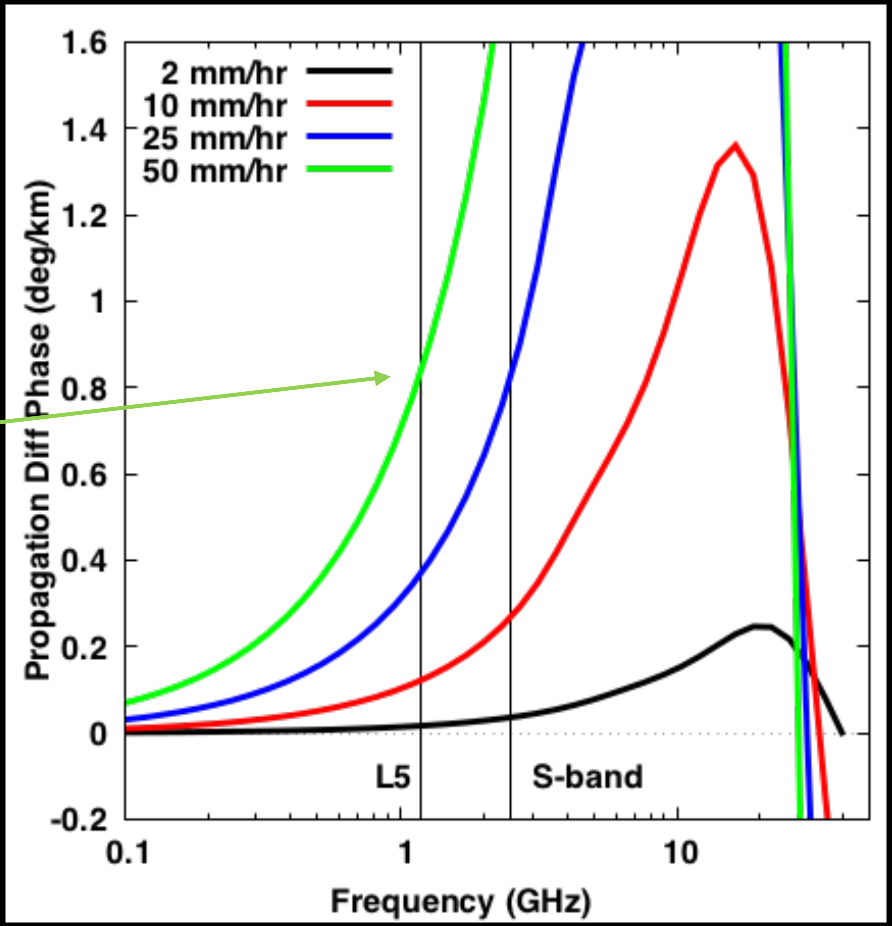

Polarimetric differential phase shift $\Delta\phi$ due to rain is a path-weighted sum =

0.35(25) + 0.1(25) + 0.8(25) + 0.05(25)= **14.5 deg= 5 mm**

This value would clearly indicate the presence of heavy precipitation somewhere along the ray path

However, different combinations of path lengths and rain intensities yield a similar phase difference

Long Heritage in Polarimetric Doppler Radar Community

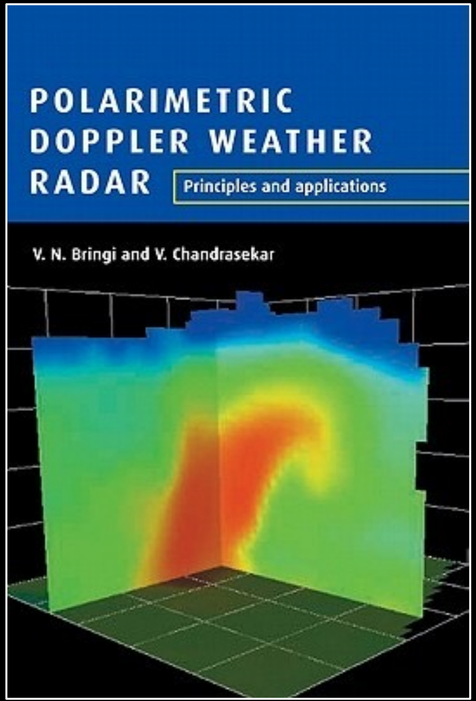

Specific differential phase shift (deg km^{-1})

forward scattering amplitudes

$$K_{DP} = \frac{180}{\lambda} \int Re(f_H - f_V)\, N(D)\, dD$$

Propagation differential phase shift (deg)

$$\phi_{DP} = 2 \int_{r_1}^{r_2} K_{DP}(r)\, dr$$

Analogous to the polarimetric RO $\Delta\phi$ measureable

N(D)= hydrometeor size distribution within each radar pulse volume

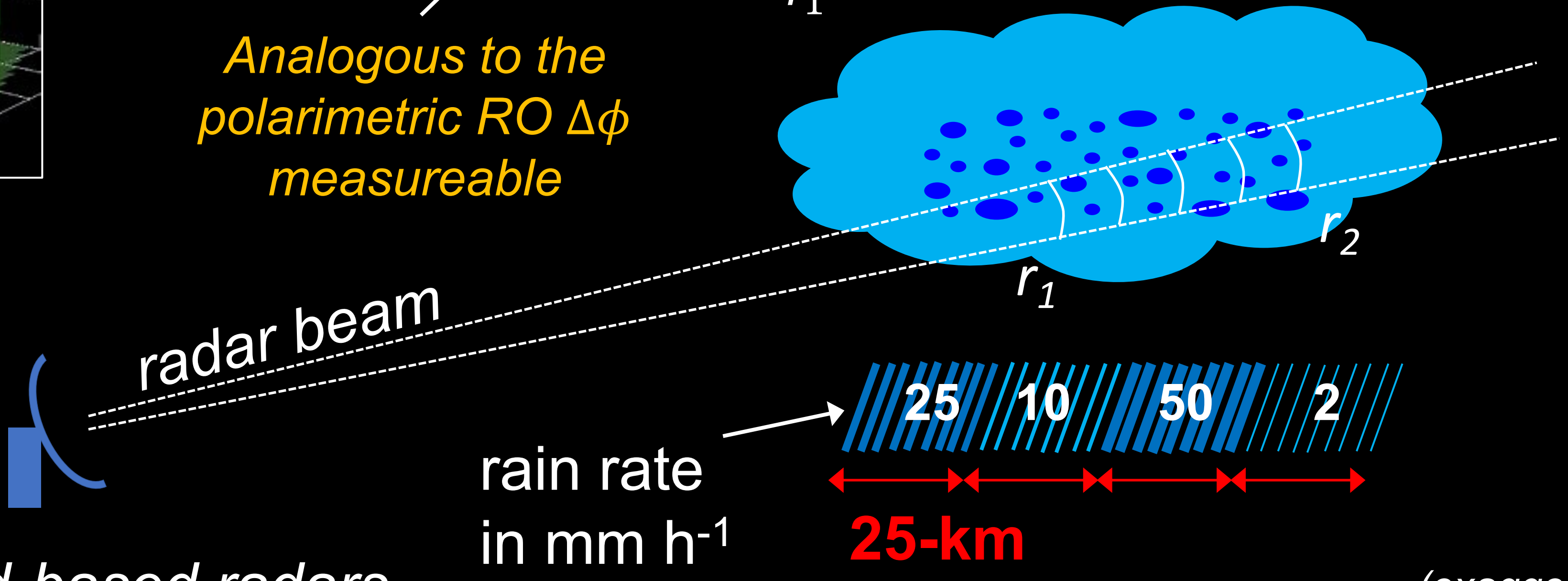

NEXRAD ground-based radars

(exaggerated depiction)

Assessing ROHP with Current GPM MW Radiometer Constellation

ROHP Cal/Val has been done to date separating data by “near-surface” precipitation from GPM-IMERG data (*Padulles et al*, 2020)

The polarimetric signal responds to the precipitation vertical structure along each ray path. Further assessment requires an observational dataset that has 3-D condensed water content structure

Very few coincidences and ray-alignments within narrow swath GPM dual-frequency radar (DPR, 240-km Ku-band swath; 240-km Ka-band after May 2019) to compare with $\Delta\phi$ profile

Use wide-swath GPM passive MW radiometer constellation (GPM/GMI, GCOM-W/AMSR-2, NPP/NOAA-20 ATMS, MetOp/MHS, DMSP/SSMIS, etc.)

Vertical profiles of the condensed water content provided by the Emissivity Principal Components (EPC) passive MW precipitation profiling algorithm, whose *a-priori* data comes from the DPR (*Utsumi et al* 2020, *Turk et al* 2018)

+/-15 min coincidences ROHP/GPM constellation passive MW → Run EPC for passive MW scans covering all RO rays from 20-km to surface → Ray-tracing along same 0.1-km level rays for ROHP → Propagate each ray through the 3-D cloud. Accumulate rain and ice water path → Simulate $\Delta\phi$ profile using rain and a few simple ice shape assumptions

Latest ROHP APC 20200513 reprocessing

Lookup tables of K_{DP} for rain (Beard et al axis ratio) and ice (several axis ratios) using T-matrix

About 8000 ROHP cases

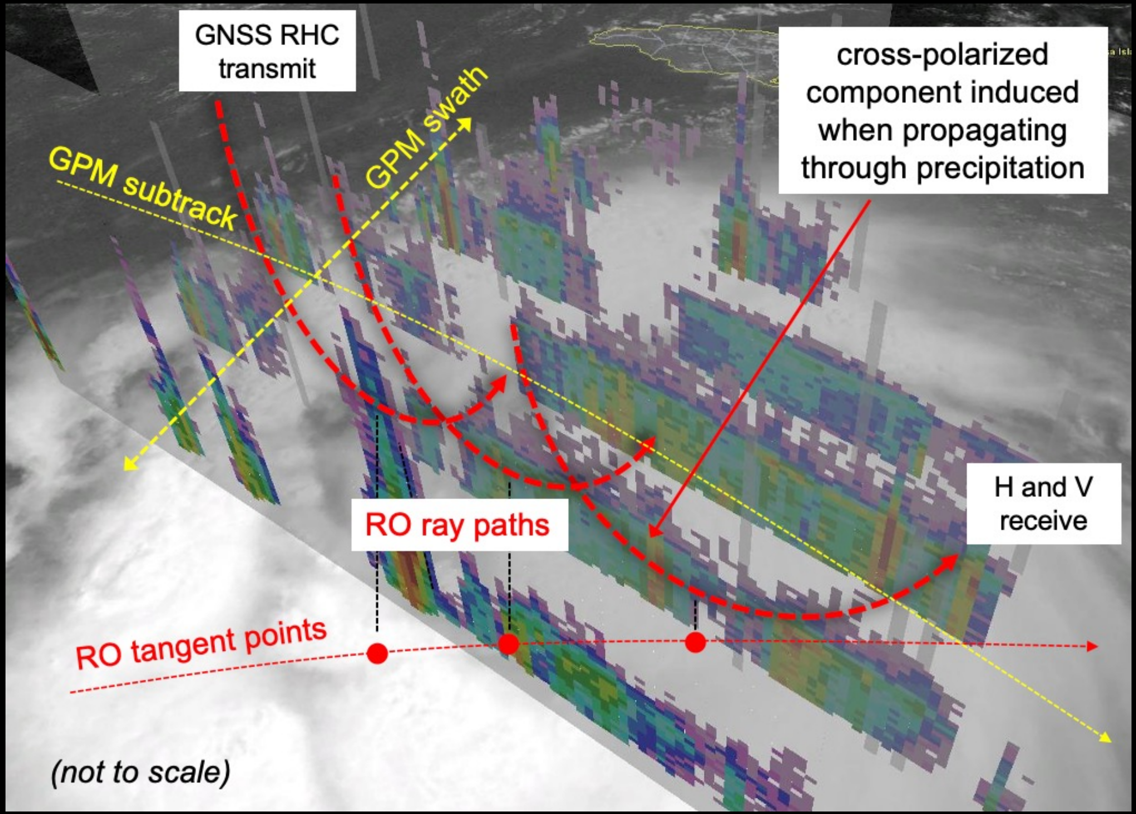

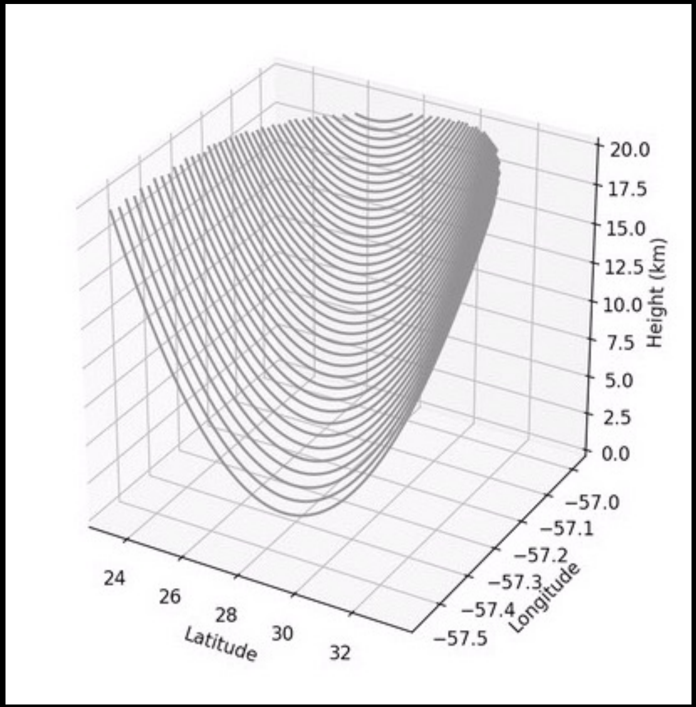

Exaggerated 3-D water content structure

ROHP 2019/04/15 0544 UTC
DMSP F-18 SSMIS 0556 UTC

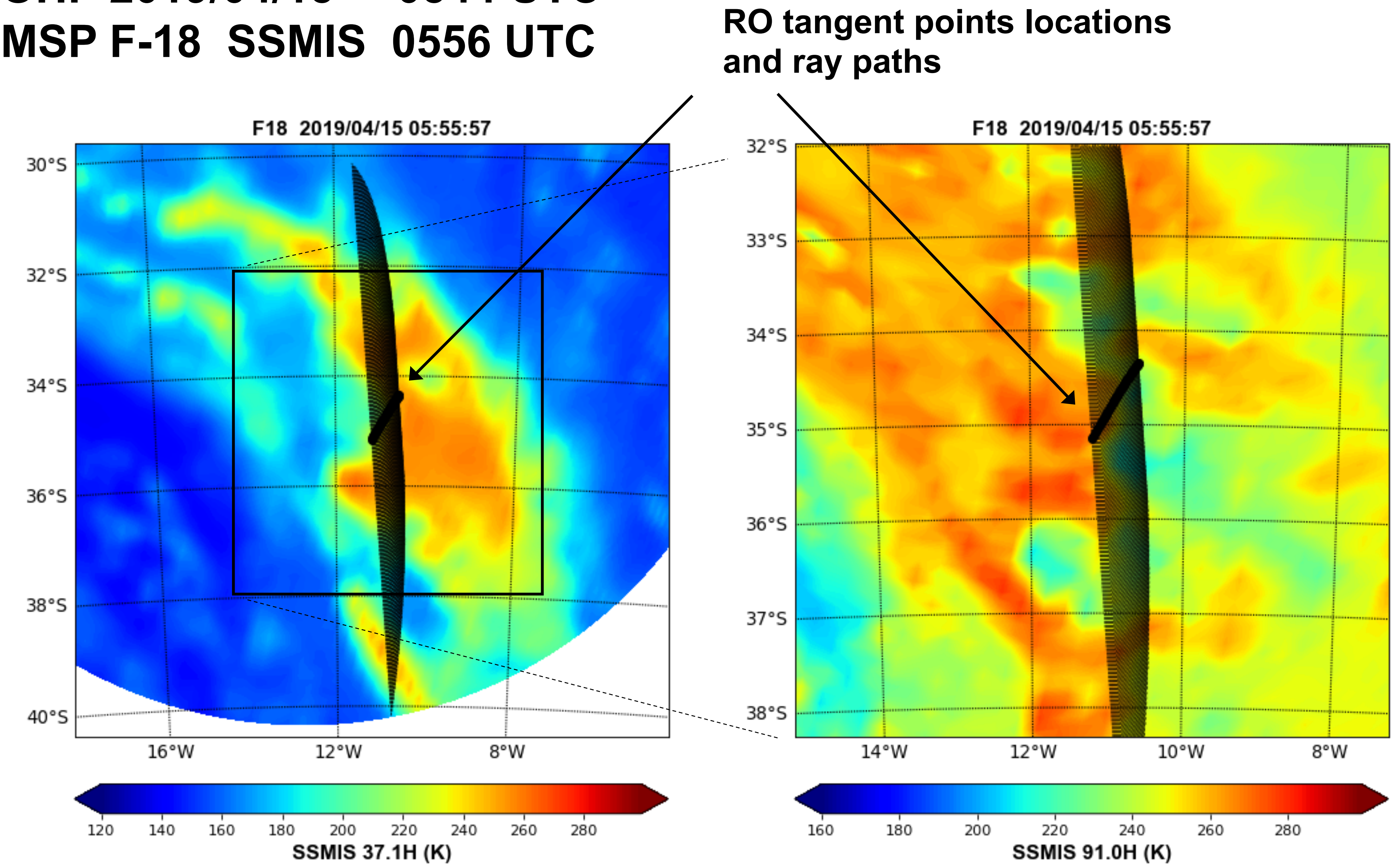

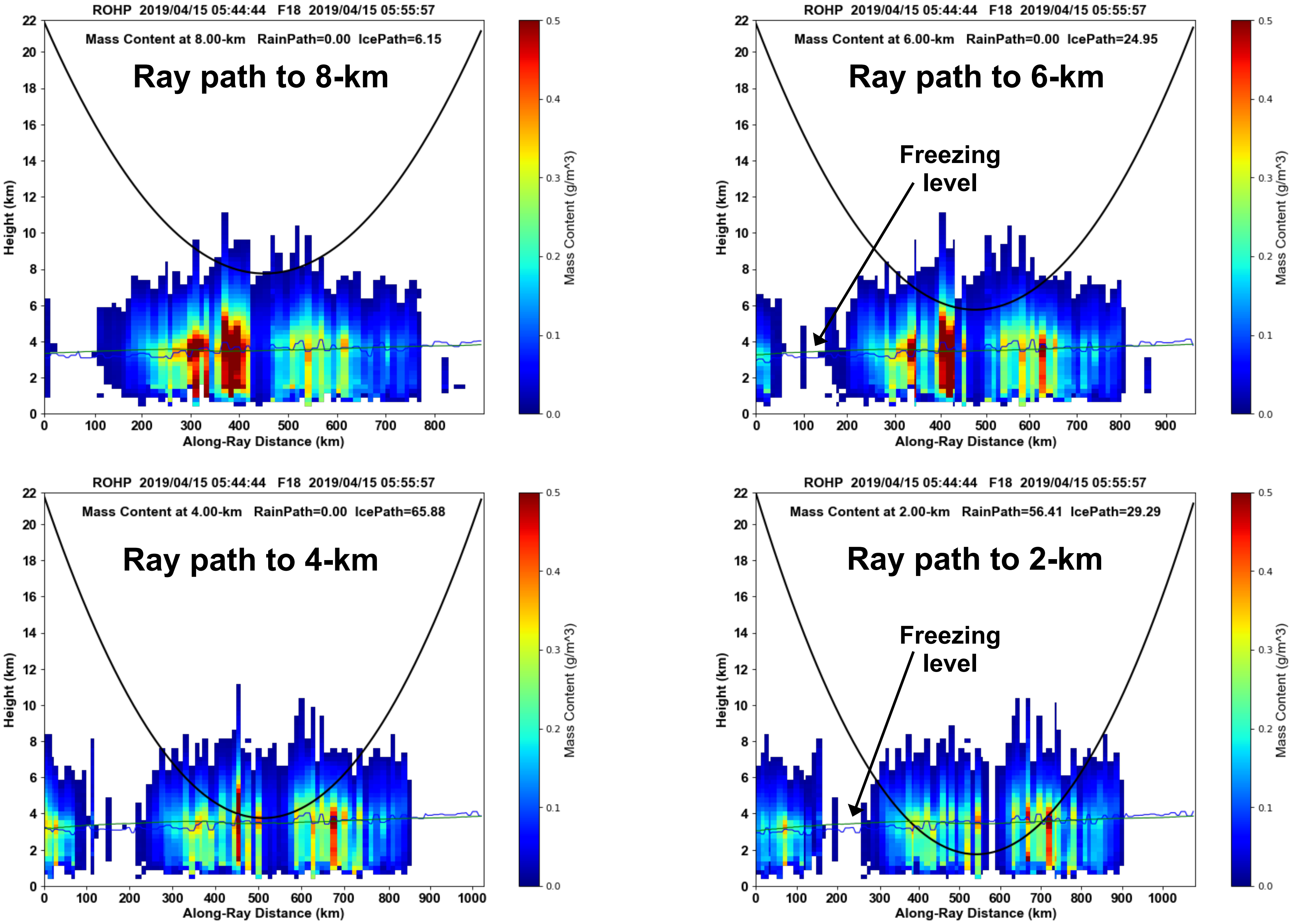
ROHP 2019/04/15 05:44:44 F18 2019/04/15 05:55:57
Mass Content at 8.00-km RainPath=0.00 IcePath=6.15
Ray path to 8-km
ROHP 2019/04/15 05:44:44 F18 2019/04/15 05:55:57
Mass Content at 6.00-km RainPath=0.00 IcePath=24.95
Ray path to 6-km
Freezing level
ROHP 2019/04/15 05:44:44 F18 2019/04/15 05:55:57
Mass Content at 4.00-km RainPath=0.00 IcePath=65.88
Ray path to 4-km
ROHP 2019/04/15 05:44:44 F18 2019/04/15 05:55:57
Mass Content at 2.00-km RainPath=56.41 IcePath=29.29
Ray path to 2-km
Freezing level
Height (km)
Along-Ray Distance (km)
Mass Content (g/m^3)

Water Path Profile
(sum along each ray)

ROHP 2019/04/15 0544 UTC
DMSP F-18 SSMIS 0556 UTC

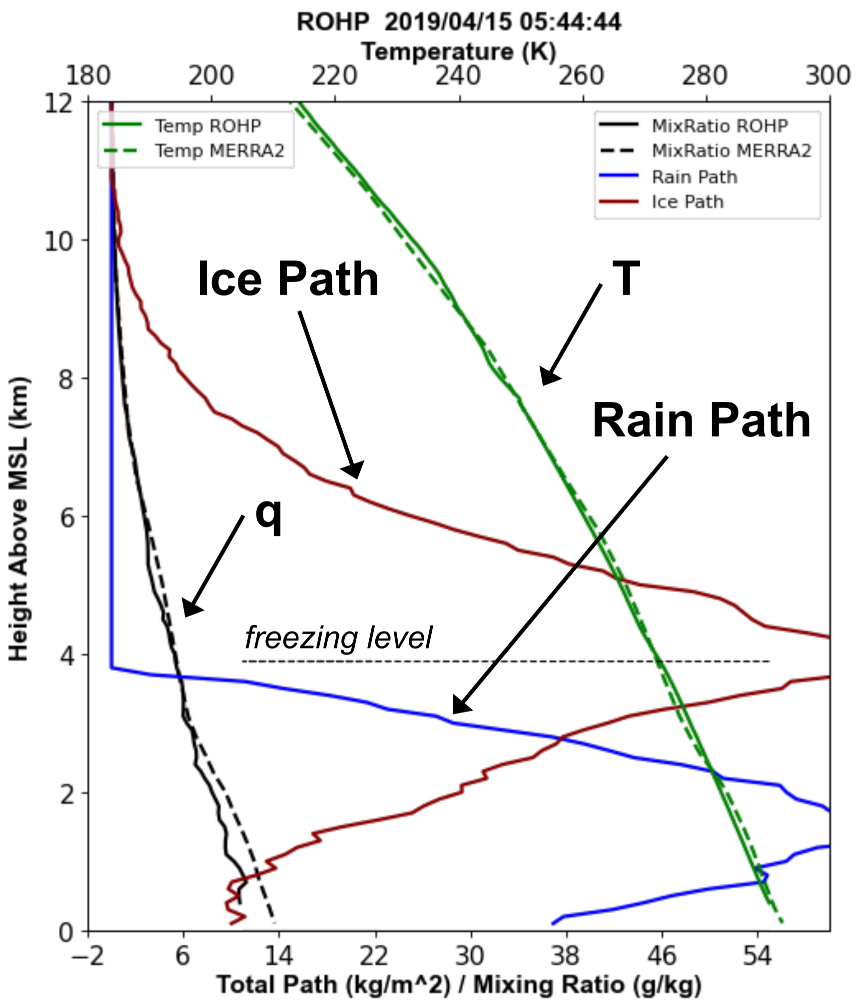

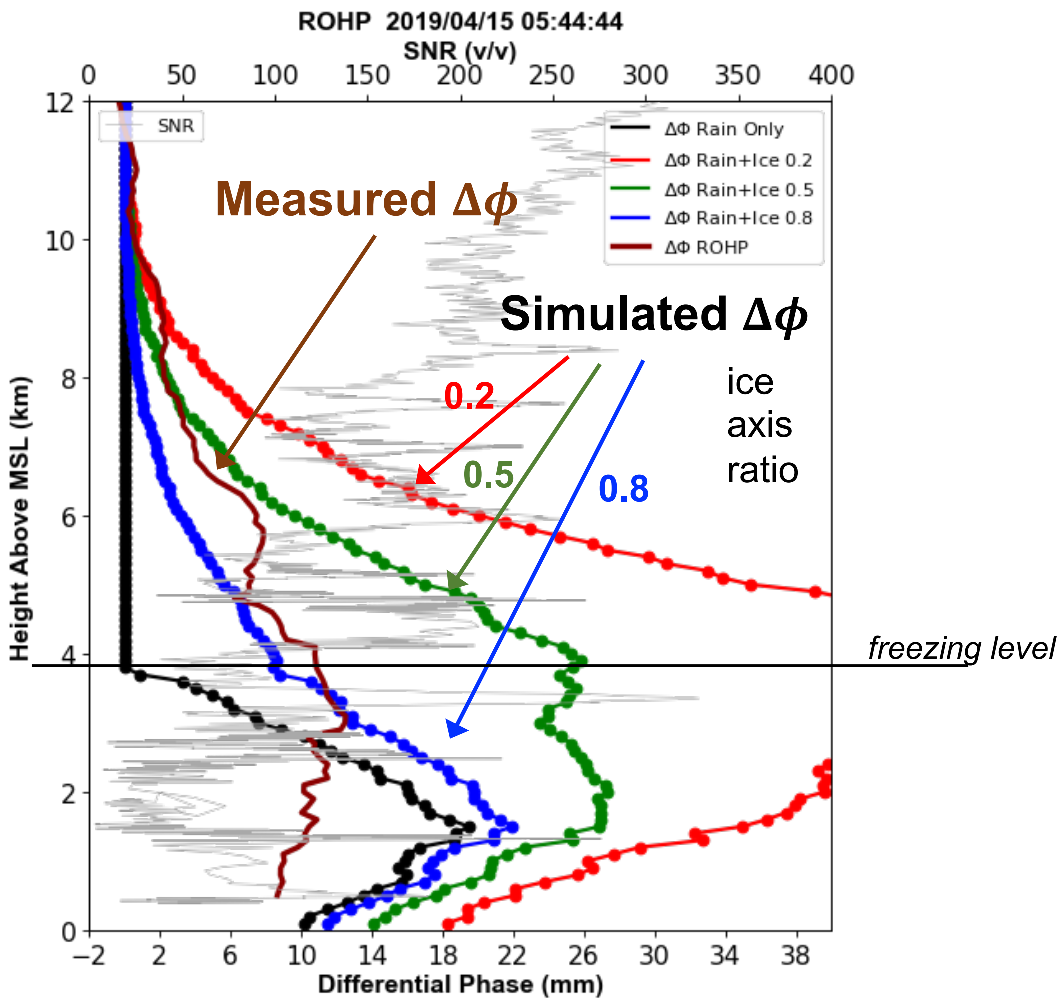

20 kg m^{-2} = 1 g m^{-3} along a 20-km path
= 0.5 g m^{-3} along a 40-km path
= 0.2 g m^{-3} along a 100-km path

← From the actual observations, same water path could occur from many different cloud conditions

Detection Characteristics: Total Rain+Ice Water Path

ROHP Rays (Passing QC)

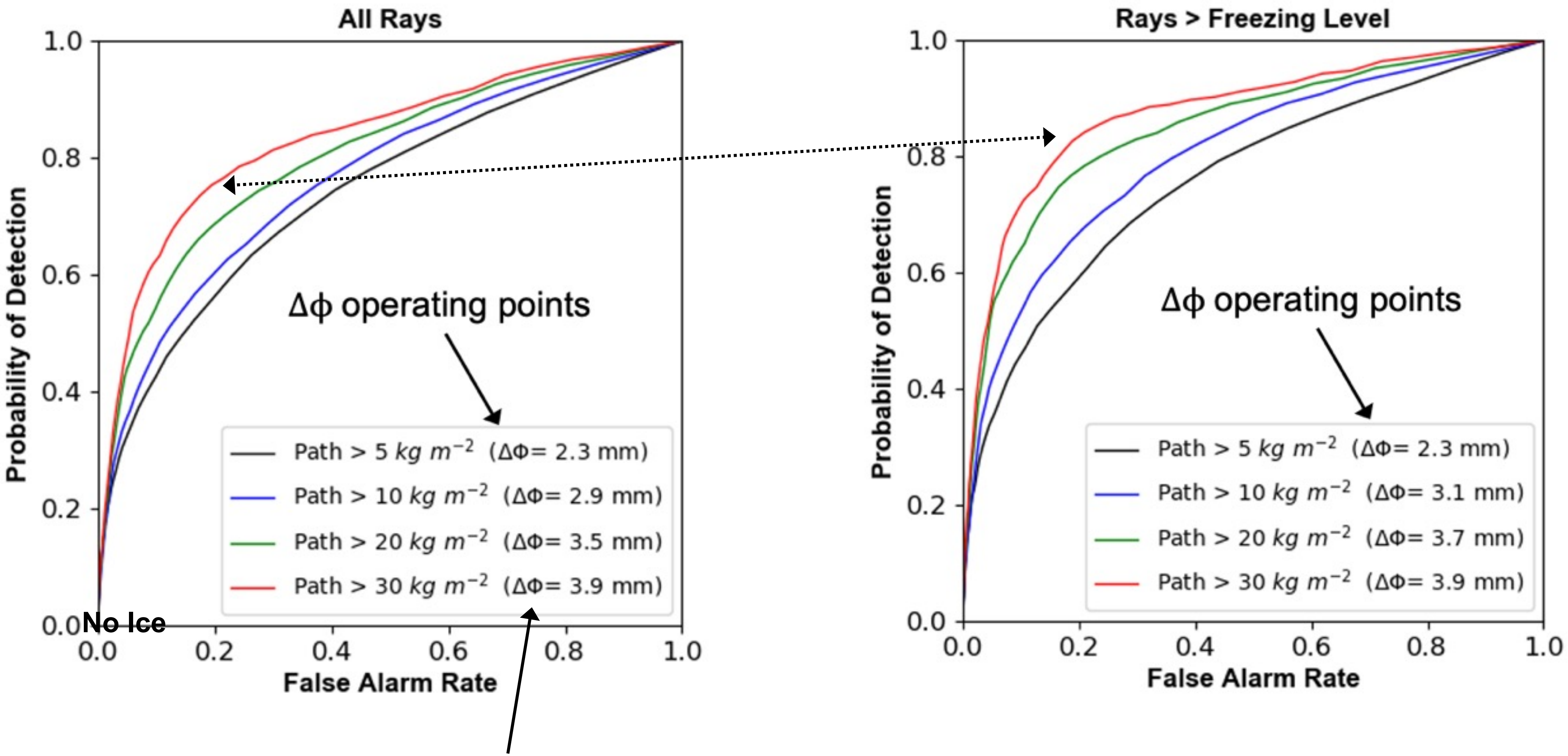

Δϕ “operating point” (balance of POD and FAR)

Better detection of total water path > freezing level

Scattering of particles – Simple prolate spheroids

Below freezing level

Beard et al 1984 axis ratio for rain DSD, parametric gamma (Haddad et al 1997)

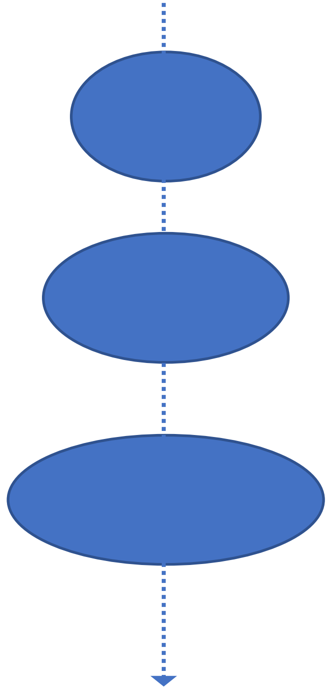

Above freezing level

Fixed axis ratio (0.8, 0.5, 0.2) for solid ice

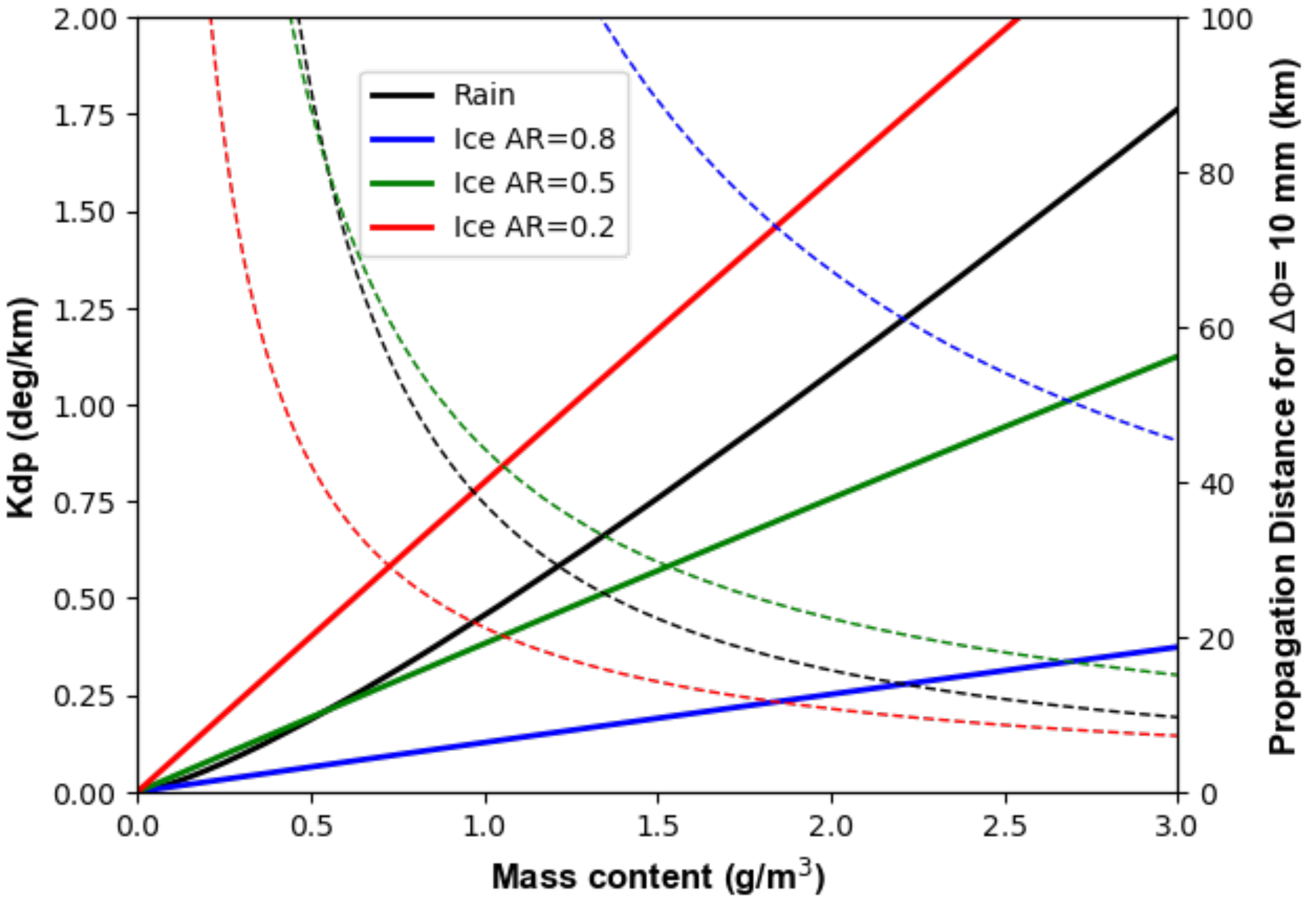

See *Padullés et al* IEEE-TGRS 2021 (also next talk right after this one)

Hydrometeor Asymmetry Characteristics

Normalized Histograms
ROHP Rays: All Rays
Total Rain+Ice Water Path

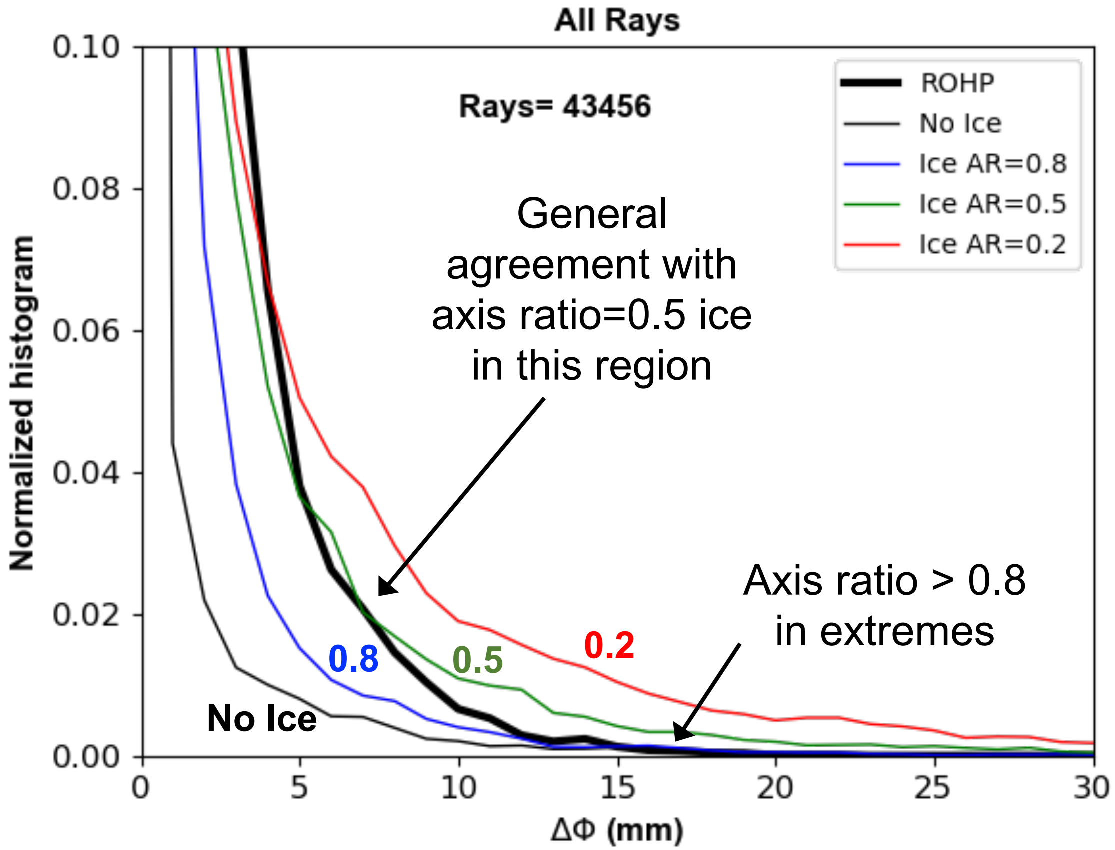

Normalized Histograms
ROHP Rays: Above Freezing Level
Total Rain+Ice Water Path

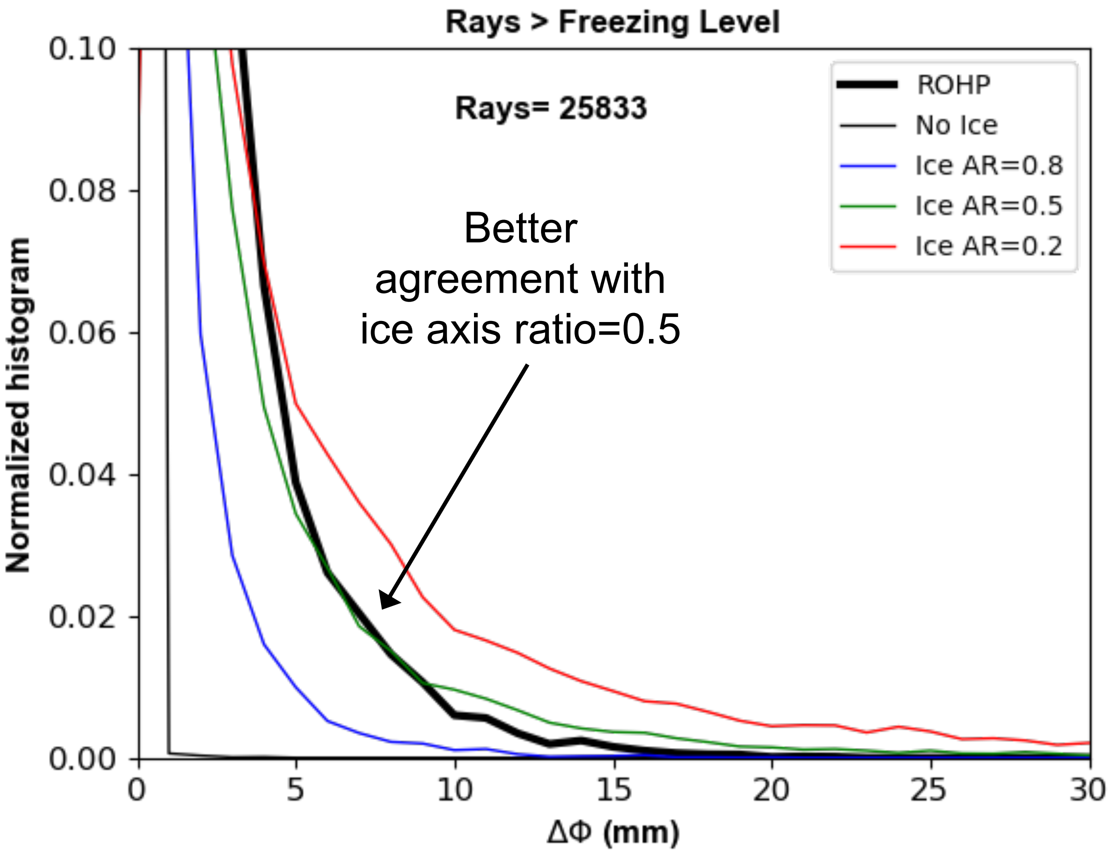

Hydrometeor Asymmetry Characteristics

Normalized Histograms
ROHP Rays: T=253K Level and Above
Total Rain+Ice Water Path

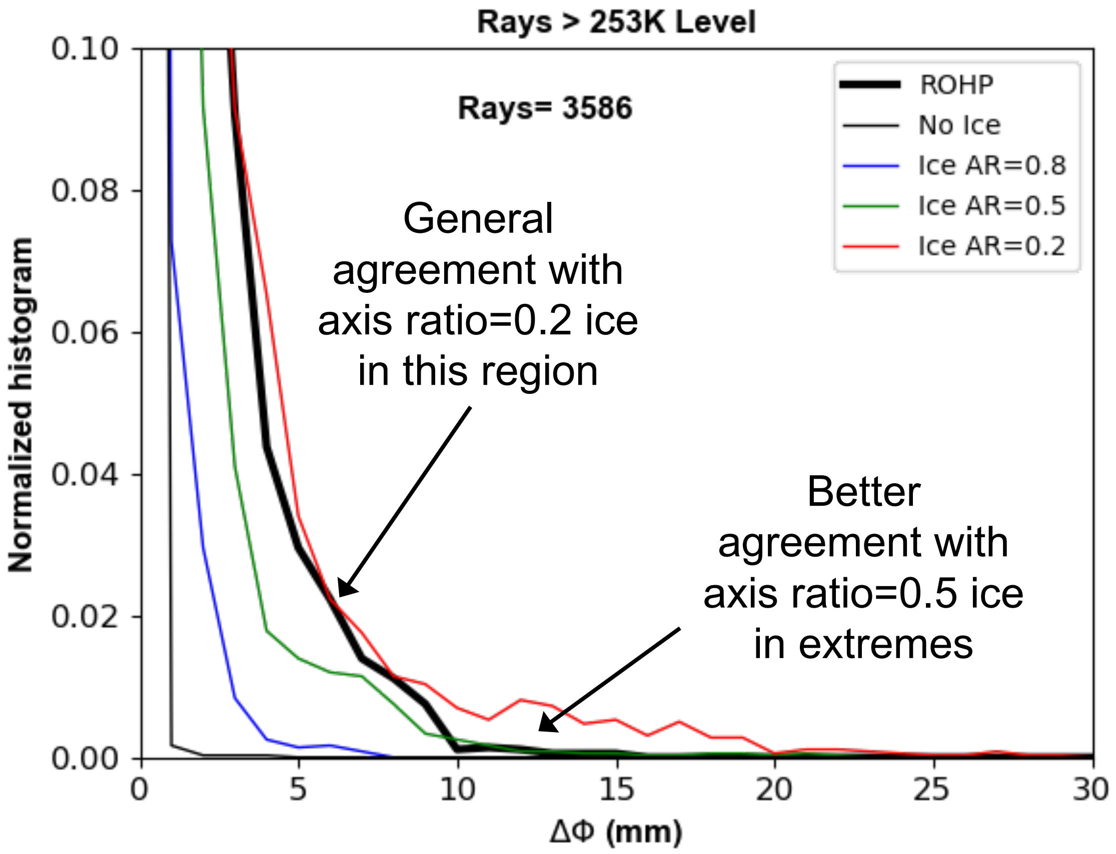

Normalized Histograms
ROHP Rays: Nearly All Rain
Total Rain+Ice Water Path

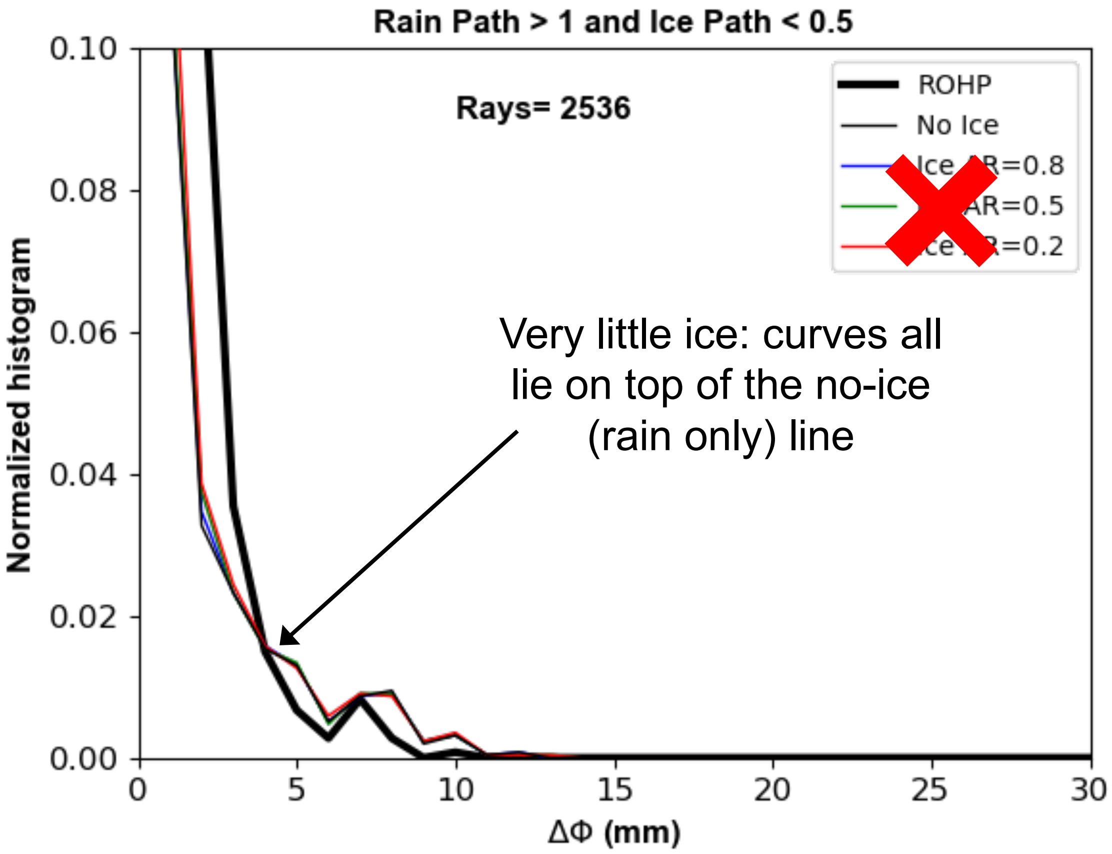

Relation to Humidity Structure

Separated by Height of Top-Most Temperature Level where Path > 1 kg m^{-2}

Separated by Height of Top-Most Temperature Level where $\Delta\phi$ > 3-mm

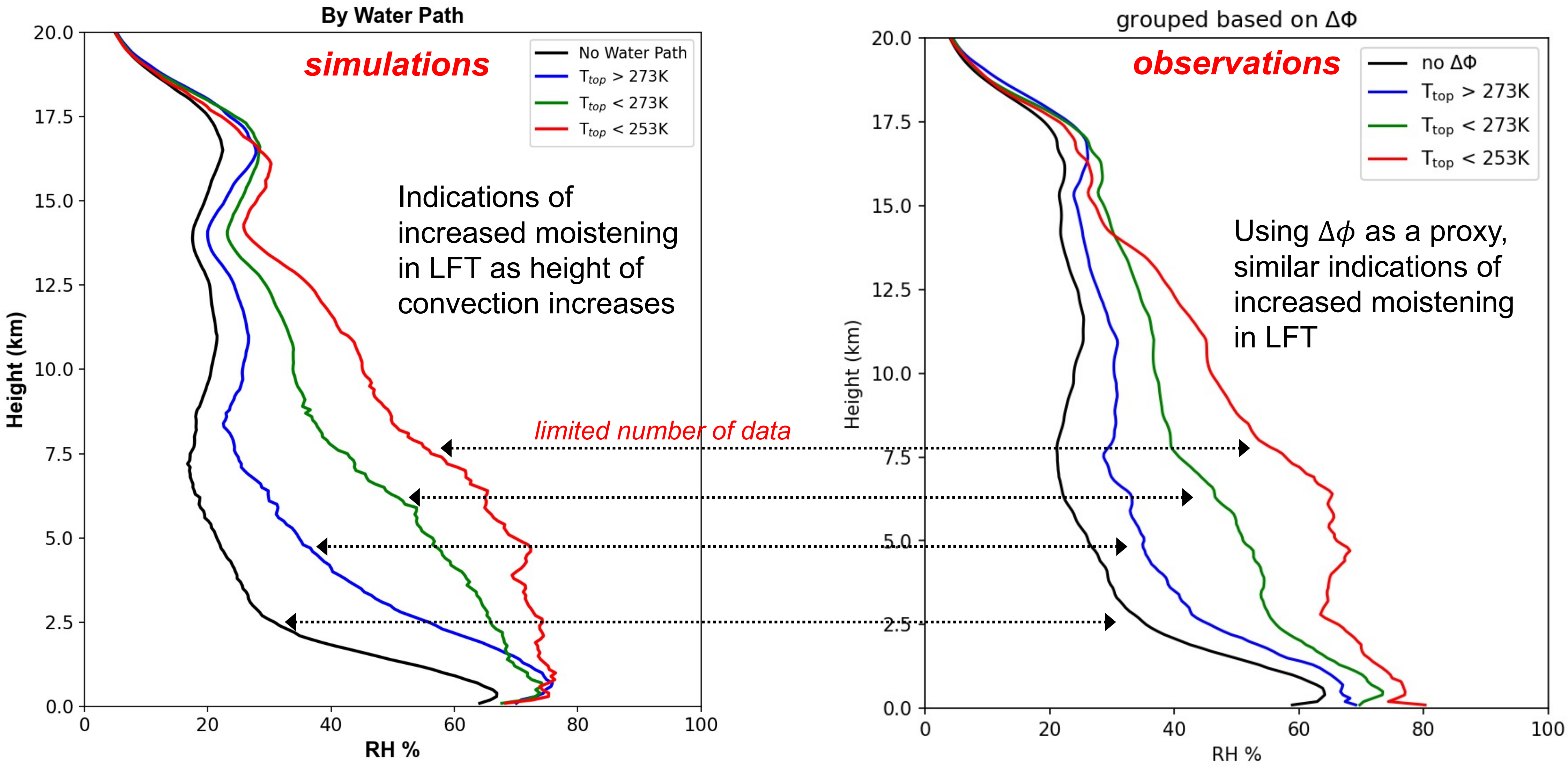

Summary

A poor man's simple forward operator was developed using passive MW profile retrievals and a ray tracing model, to compare a large number of simulated and observed $\Delta\phi$ profiles

Even with perfect knowledge of the microphysics, cloud geometry relative to each ray is important to interpret (and simulate) the $\Delta\phi$ profile - challenging to accurately forward model

Therefore, the relation between $\Delta\phi$ and the total condensed water path was performed on a collective basis using detection statistics. FAR < 0.2 for total water path > 20 kg m^{-2}, esp. for rays that don't fall below the freezing level height

Overall "qualitative agreement" with range of axis ratio of precipitation-sized ice phase hydrometeors noted by others (eg Matrosov et al 2005), and "rain-only" rays

Using $\Delta\phi$ as a proxy for convection, sensitivity of precip to vertically-resolved moisture?

PAZ data are openly available, investigations and collaborations welcomed

https://paz.ice.csic.es

Recent Publications

Padullés, R., Cardellach, E., Turk, F.J., Ao, C.O., Juárez, M. de la T., Gong, J., Wu, D.L., 2021. Sensing Horizontally Oriented Frozen Particles With Polarimetric Radio Occultations Aboard PAZ: Validation Using GMI Coincident Observations and Cloudsat a Priori Information. *IEEE Transactions on Geoscience and Remote Sensing*, accepted. https://doi.org/10.1109/TGRS.2021.3065119

Utsumi, N., Turk, F.J., Haddad, Z.S., Kirstetter, P.-E., Kim, H., 2020. Evaluation of precipitation vertical profiles estimated by GPM-era satellite-based passive microwave retrievals. *J. Hydrometeor*, 22, 95-112 . https://doi.org/10.1175/JHM-D-20-0160.1

Gong, J., Zeng, X., Wu, D.L., Munchak, S.J., Li, X., Kneifel, S., Ori, D., Liao, L., Barahona, D., 2020. Linkage among ice crystal microphysics, mesoscale dynamics, and cloud and precipitation structures revealed by collocated microwave radiometer and multifrequency radar observations. *Atmospheric Chemistry and Physics* 20, 12633–12653. https://doi.org/10.5194/acp-20-12633-2020

Padullés, R., C.O. Ao, F.J. Turk, and M. de la Torre-Juárez, B.A. Iijima, K.N. Wang, E. Cardellach, 2019. Calibration and Validation of the Polarimetric Radio Occultation and Heavy Precipitation experiment Aboard the PAZ Satellite. *Atmos. Meas. Techniques*, https://doi.org/10.5194/amt-2019-237

Cardellach, E., S. Oliveras, A. Rius, S. Tomás, C.O. Ao., G.W. Franklin, B.A. Iijima, D. Kuang, T. Meehan, R. Padullés, F.J. Turk, et al., 2019. Sensing Heavy Precipitation with GNSS Polarimetric Radio Occultations. *Geophysical Research Letters*, *46*, 1024–1031. https://doi.org/10.1029/2018GL080412

Turk, F.J.; Padullés, R.; Ao, C.O.; Juárez, M.T.; Wang, K.-N.; Franklin, G.W.; Lowe, S.T.; Hristova-Veleva, S.M.; Fetzer, E.J.; Cardellach, E.; Kuo, Y.-H.; Neelin, J.D., 2019. Benefits of a Closely-Spaced Satellite Constellation of Atmospheric Polarimetric Radio Occultation Measurements. *Remote Sens.*, *11*, 2399. https://doi.org/10.3390/rs11202399

Padullés, R., Cardellach, E., Wang, K. N., Ao, C. O., Turk, F. J., and de la Torre-Juárez, M., 2018. Assessment of GNSS radio occultation refractivity under heavy precipitation, *Atmospheric Chemistry and Physics,* https://doi.org/10.5194/acp-2018-66.

Juárez, M. de la T., R. Padullés, F.J. Turk, and E. Cardellach, 2018: Signatures of Heavy Precipitation on the Thermodynamics of Clouds Seen From Satellite: Changes Observed in Temperature Lapse Rates and Missed by Weather Analyses. *J. Geophys. Res: Atmospheres*, *123*, 13033-13045. https://doi.org/10.1029/2017JD028170

Tomás, S., Padullés, R. & Cardellach, E., 2018. Separability of Systematic Effects in Polarimetric GNSS Radio Occultations for Precipitation Sensing. *IEEE Transactions on Geoscience and Remote Sensing* **56**, 4633–4649. https://doi.org/10.1109/TGRS.2018.2831600

Cardellach, E., Padullés, R., Tomás, S, Turk, F. J., Ao, C. O., and de la Torre-Juárez, M., 2017. Probability of intense precipitation from polarimetric GNSS radio occultation observations, *Q. J. Royal Meteorological Soc*iety, 12. https://doi.org/10.1002/qj.3161

Padullés, R. Cardellach, E. de la Torre Juárez, M., Tomas, S., Turk, F. J., Oliveras, S., Ao, C. O. and Rius, A., 2016. Atmospheric polarimetric effects on GNSS Radio Occultations: the ROHP-PAZ field campaign, *Atmospheric Chemistry and Physics*, 16, 635-649, https://doi.org/10.5194/acp-16-635-2016.

Cardellach, E., Tomás, S., Oliveras, S., Padullés, R., Rius, A., De la Torre-Juárez, M., Turk, F.J., Ao, C.O., Kursinski, E.R., Schreiner, B., Ector, D. and Cucurull, L., 2014. Sensitivity of PAZ LEO Polarimetric GNSS Radio-Occultation Experiment to Precipitation Events, *IEEE Trans. Geoscience and Remote Sens.*, 53,190-206, http://doi.org/10.1109/TGRS.2014.2320309